



# Beyond the surface: Coupling water permeability assessments to X-ray micro-computed tomography for evaluation of self-healing on lime-based mortars

Franco Grosso Giordano<sup>a,d,\*</sup>, Dulce Valdez Madrid<sup>b</sup>, Laurenz Schröer<sup>b</sup>, Nico Boon<sup>a</sup>,  
Veerle Cnudde<sup>b,c</sup>, Nele De Belie<sup>d</sup>

<sup>a</sup> Ghent University, Center for Microbial Ecology and Technology (CMET), Coupure Links 653, Ghent B-9000, Belgium

<sup>b</sup> Ghent University, Dept. Geology, Krijgslaan 281/Building S8, Ghent B-9000, Belgium

<sup>c</sup> Utrecht University, Dept. of Earth Sciences, Princetonlaan 8a, Utrecht 3584, Netherlands

<sup>d</sup> Ghent University, Magnel-Vandepitte Laboratory, Dept. of Structural Engineering and Building Materials, Technologiepark Zwijnaarde 60, Ghent B-9052, Belgium

## ARTICLE INFO

### Keywords:

Self-healing

Lime-based

Mortar

X-ray micro-computed tomography (micro-CT)

Material characterization

## ABSTRACT

Self-healing, a promising solution to cementitious structures' main problem – cracking, involves complex dynamics influenced by factors like crack type, size, and binder material. Existing tests lack a comprehensive approach to describe it. This study coupled the results of X-ray micro-computed tomography (micro-CT) to water flow tests and optical microscopy to obtain 3D crack volume analysis, water permeability, and crack widths, respectively. Three binder formulations - a pure cement, a 50 % lime – 50 % cement and a 33 % lime - 67 % metakaolin mix - were selected to test the method's accuracy across different mortars. On average, pure cement samples exhibited the best healing efficiency in all tests, albeit not significantly. Interestingly, neither water flow nor microscopy measurements could be correlated to crack volume changes, suggesting different aspects of self-healing were captured. Micro-CT analysis provided clarification, revealing that self-healing predominately occurred at the surface. Additionally, the precipitation of self-healing products at the pore-crack interface led to certain pores becoming disconnected from the original crack. Therefore, the measured volume change of the crack appeared to be larger than the actual precipitation of healing products. Given the different limitations encountered on all tests, the use of coupled tests is encouraged for future studies.

## 1. Introduction

Self-healing of cementitious materials has seen an exponential growth as a research topic over the last 20 years [1–3]. This interest has risen with the need of decarbonization of the cement industry and the need for longer lasting cementitious materials with lower carbon footprints. Multiple reviews exist that explore the modifications that can promote self-healing, such as bacterial additives [4], microcapsules [5], crystalline admixtures [6] and superabsorbent polymers (SAPs) [7]. Despite that cementitious materials are ubiquitous to the construction industry, new alternatives are also being explored such as geopolymers [8] and other lesser studied binder types, including lime-based materials [9,10].

Previous work on self-healing has demonstrated that the capacity of autogenous healing of any material is tied to a variety of parameters that

influence the progress of healing such as crack width, crack geometry, rugosity and binder composition. Thus, it is necessary to have a comprehensive understanding of these parameters. Usually, single techniques do not fully illustrate the whole process of healing. 2D techniques such as optical microscopy do not provide insights into the extent of healing through a whole crack. To study the inside of a specimen then, often a destructive approach is required, but this is not desired if multiple testing stages are needed. Due to the limitations of optical microscopy, durability tests that can provide quantification of the healing progress have been developed. These generally include different types of permeability tests and tests of regain in mechanical properties [2,11]. However, durability tests cannot offer descriptive assessments of the healing occurring within the specimens. This information is nonetheless essential to be able to discern the effectiveness of healing, such as where the formation of healing products is happening

\* Corresponding author at: Ghent University, Center for Microbial Ecology and Technology (CMET), Coupure Links 653, Ghent B-9000, Belgium.  
E-mail address: [franco.grossojiordano@ugent.be](mailto:franco.grossojiordano@ugent.be) (F. Grosso Giordano).

<https://doi.org/10.1016/j.conbuildmat.2024.136603>

Received 7 December 2023; Received in revised form 5 May 2024; Accepted 9 May 2024

Available online 15 May 2024

0950-0618/© 2024 Elsevier Ltd. All rights reserved, including those for text and data mining, AI training, and similar technologies.

and to what extent.

X-ray micro-computed tomography (micro-CT) [12,13] has been hailed as a promising technique for the study of self-healing due to its capacity to overcome the limitations stated above, while at the same time it is capable of performing both qualitative and quantitative assessments in a non-destructive manner. Snoeck et al. [14], used it to study the capacity of SAPs to improve self-healing in cement mortars and could quantify the amount of healing products generated by the addition of SAPs. They also showed that this precipitation of healing products extended to the pore network. Van Stappen et al. [15], then demonstrated that micro-CT offers a tool to study the distribution and debonding of microcapsules used for self-healing. They argued that intrusive techniques such as optical or electron microscopy can lead to rupture of the microcapsules and indications of healing when there is none. Similarly, Sidiq et al. [16] studied different concentrations of microcapsules and their effect on the healing of a crack. Despite that the addition of larger amounts of microcapsules led to better healing, micro-CT allowed them to confirm that extra additions also hindered bond strength of the matrix with aggregates as the microcapsules reduced hydration. Kontiza et al. [17] also studied microcapsules in cementitious materials although they used micro-CT merely to determine whether their production technique resulted in successful embedding of the microcapsules. Meanwhile, Fan and Li [18] explored the addition of fly-ash to Portland cement, and used micro-CT to study the progress of self-healing on multiple time points and cracks in the same sample. Still, limitations were encountered in these works particularly when it comes to the resolution of the images of the samples. For these reasons, Wang et al. [19], who used micro-CT to study bacterial additives for self-healing, stressed the need to perform micro-CT analysis together with other techniques such as electron microscopy.

It is necessary to study self-healing dynamics through a more holistic approach in which multiple techniques are combined. Although different testing methods are used in previous work, these have always been applied on different test series due to the ease of managing samples, the destructive nature of the testing techniques and shape and size requirements for some techniques. Coupled experiments that demonstrate the quantitative and qualitative effect of the healing processes on a single sample are not common due to their technical complications. Few studies, like that of Fukuda et al. [20], have corroborated whether micro-CT was in good agreement with real observations in the same sample. Fukuda et al. [20] used Scanning Electron Microscopy (SEM) to study a region on the surface of the sample and concluded that they got more robust results that would be hard to achieve if they had relied on the preparation of multiple specimens that compromise reproducibility.

Here, the first study is performed to evaluate self-healing by coupling results of microscopy, water permeability tests and micro-CT obtained on the same specimen. Whereas microscopy and water permeability are commonly used techniques to assess self-healing, micro-CT is less used. Nevertheless, the former techniques cannot provide insight into what is occurring within samples. As such, the aim of this work was to use micro-CT scans that visualized the whole crack before and after healing, to study how microscopy and water flow test reflect changes to the internal structure. At the same time, this is applied on standard-sized specimens, which are more representative of healing dynamics than smaller sized specimens previously used in most self-healing research using micro-CT. Three mortar mixes of varying strengths were chosen to evaluate the effectiveness of the method as a universally applicable test in a range of self-healing materials. Two different lime-based formulations, a 50 % lime – 50 % cement and a 33 % lime - 67 % metakaolin mixture were tested and compared to a cement mixture. The healing efficiencies obtained in each test were calculated and three samples were chosen for an in-depth characterization using the micro-CT scans. Furthermore, to our current knowledge this is the first time self-healing has been reported in a lime-pozzolanic mixture and full crack dynamics are discussed for a lime-based mortar, which remains a largely understudied material when compared to cement-based mortars.

## 2. Materials and methods

### 2.1. Materials

#### 2.1.1. Mix design

Three mortar formulations were designed of cement CEM II A/L 32.5 R (Tarmac, United Kingdom), hydrated lime CL 90-S (Lhoist, Belgium) and metakaolin Metapor (Poraver, Germany). These were a pure cement binder (C100L0), a 50–50 by volume cement-lime mixture (C50L50) and a 33–67 by volume metakaolin-lime mixture (M33L67), with a binder-to-aggregate ratio of 1:3 by volume. The bulk densities of cement, lime and metakaolin were 964 kg/m<sup>3</sup>, 405 kg/m<sup>3</sup> and 296 kg/m<sup>3</sup>, respectively. The water-to-binder (w/b) ratio was determined in accordance with EN 1015–2, to reach a flow of 175 ± 10 mm (Table 1). The chemical composition and particle sizes of the binders can be found in Table 2 and Table 3, respectively.

#### 2.1.2. Sample preparation

The samples were designed by adapting Van Mullem et al. [21]'s active crack control and water permeability test to cylindrical samples. Nine samples per mortar composition were cast in 50 × 45 mm (height x diameter) PVC cylinders with one side sealed with epoxy resin. A cast-in-hole of 5 mm was created using a very well-oiled reinforcement bar that traverses the sample horizontally at the half (Fig. 1) which would be the inlet through which water would flow during the water permeability tests. Mortar mixes were prepared and cured in accordance with EN 1015–11 standard for masonry mortars. Accordingly, a double layer of gauze, 6 layers of filter paper and a 5 kg load were placed on the exposed surface of M33L67 samples, which exceed the 50 % lime content, for 3 h after casting.

Samples were cured for 2 days in the case for cement- or 5 days for metakaolin-containing mixtures (which showed slower hardening), at 95 % relative humidity (RH) and room temperature (RT) of 20 °C. Then, they were demoulded, the reinforcement bar removed and left to cure further until 7 days of age at 95 % RH and RT of 20 °C. At day 7, the first 10 mm of the cast-in-hole was enlarged to 6 mm diameter and plastic tubing was inserted and glued. This tubing would be used to connect the samples to the water flow setup. The opposite side of the cast-in-hole was sealed with silicone to prevent leakage. Samples were wrapped in duct tape and split with a Brazilian splitting test to create a crack perpendicular to the cast-in-hole. The duct tape ensured the two halves remained together and did not shift. To ensure the same sizes of cracks in all specimens the crack width was adjusted using two plastic hose clamps to reach ~300 µm at the widest part. The adjusted side was the top side of the sample where the crack mouth was located. Aluminium tape was placed on the crack opening in the bottom side of the cylinder, which was not studied, to ensure leakage during water flow tests occurred only through the exposed crack opening at the top face. Epoxy was then used to cover the vertical crack openings on the circumference of the cylinder to further ensure water tightness. The epoxy glue was left to dry for 24 h.

### 2.2. Methods

#### 2.2.1. Experimental workflow

Three of the nine samples per mortar composition with the most

**Table 1**

Mix composition by mass and water/binder (w/b) ratio. All formulations had a binder:aggregate ratio of 1:3 by volume.

Binder composition	Total cement by mass (g)	Total metakaolin by mass (g)	Total lime by mass (g)	w/b (mass)
C100L0	289	0	0	0.7
C50L50	125	0	65	1.07
M33L67	0	28	86	1.91

**Table 2**

Chemical composition of each binder as provided by their respective manufacturers.

Constituent	Cement	Metakaolin	Lime
CaO	66 %	7–11 %	> 80 %
MgO	0.8 %	0–5 %	< 5 %
CaO + MgO	-	-	> 90 %
SiO <sub>2</sub>	16 %	70–75 %	-
Na <sub>2</sub> O	0.08 %	10–15 %	-
Al <sub>2</sub> O <sub>3</sub>	4 %	0.5–5 %	-
SO <sub>3</sub>	2.5 %	-	< 2 %
K <sub>2</sub> O	0.4 %	0–4 %	-
Fe <sub>2</sub> O <sub>3</sub>	3 %	-	-
Cl <sup>-</sup>	0.04 %	-	-
CO <sub>2</sub>	-	-	< 4
H <sub>2</sub> O	-	-	< 2 %

**Table 3**

Particle size distribution by laser diffraction from binders tested.

Material	d10		d50		d90	
	Average [μm]	COV [%]	Average [μm]	COV [%]	Average [μm]	COV [%]
CEM II-A/L 32.5 R	1.7	1.9 %	10.6	3.4 %	34.3	2.6 %
Metakaolin	3.0	3.4 %	7.9	1.4 %	16.8	0.9 %
CL90S	2.5	0.9 %	6.4	1.3 %	16.7	2.2 %

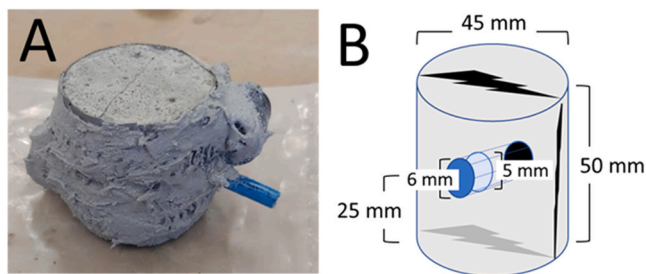


**Fig. 1.** Picture (A) and schematic drawing (B) of samples used in this study.

similar crack widths were chosen. Crack widths were first measured, and samples were placed under water for 24 h before testing water flow as described below. After testing, the samples were left to dry for 24 h. The samples were then scanned with micro-CT. After scanning, all samples were placed under water for 28 days to stimulate healing. Each formulation was located in a different container and tap water was used in all cases. After 28 days the samples were allowed to dry for 24 h and crack widths were measured again. The samples were then scanned a second time with micro-CT. Lastly, samples were placed under water for 24 h before performing a second round of water flow tests.

### 2.2.2. Microscopy

Crack widths at the crack mouth were measured using an optical microscope (Leica DMC 2900). Three regions of interest (ROIs) free of irregularities on each crack were photographed and 30 measurements per ROI were taken. The average width of the crack was calculated from the average width of each zone.

### 2.2.3. Water flow tests

Crack width measurements are a simple but effective way of showing the healing capacity of mortars at the surface. Nonetheless, it does not provide insight into the durability of the precipitated healing products. In this work, water permeability tests were chosen due to their non-destructive nature, in particular water flow tests, which have short testing times and high accuracy [22].

Briefly, the mortar samples were submerged in water for 24 h prior to testing for water permeability. This pre-treatment ensured no air remained in the sample which could affect the continuous flow of water during the test. Afterwards, the cylindrical samples were gripped with a stand and clamp with the opening side facing downwards at a height of 20 cm from a measuring scale. A hose connected the tubing on the cylinder to a closed water reservoir 30 cm above. When the test started, the reservoir was opened and water flowed from the reservoir through the tubing finally passing through the crack in the cylinder. The flowing water was collected on a container placed on top of the measuring scale and the weight of water was measured over time. Water was allowed to flow for 30 s prior to measuring to remove remaining entrapped air and weight measurements were taken every 30 s for 5 minutes (10 times in total). After the test, the samples were placed under water again to prevent air bubbles from being entrapped in the crack until the sample was measured again. All samples were measured three times.

### 2.2.4. X-ray micro-computed tomography (micro-CT)

Three samples per formulation with a size of 50 × 45 mm (height × diameter) were scanned by micro-CT at a voxel size of 30 μm (180 kV, 30 W, exposure time 750 ms) using the CoreTOM scanner (TESCAN) at Ghent University's UGCT facilities. The samples were placed on a rotating stage between an X-ray source and X-ray detector. The samples were scanned using a 1 mm aluminum filter, and 2783 projections were obtained of a 360° scan of the cylindrical sample. The same acquisition and reconstruction parameters were used for the scans before and after healing to allow comparison between scan dates. After scanning, the scans were reconstructed using the Panthera 1.4.4 software by TESCAN XRE, and this yielded a reconstructed volume with 1873 slices of 1855 × 1855 voxels. All scans can be found in the YODA repository of Utrecht University (link under construction). Further volume analysis was performed on the image analysis software Avizo 2020.3.

### 2.2.5. Volume analysis

After scanning and reconstructing the samples, Avizo 2020.3 was used to study the effects of healing on the crack volume. First, the before (date 0) and after healing (date 28) 3D volumes were aligned, taking the main crack as a reference for the resampling. Second, the segmentation of the pores in the before and after healing volumes was performed using a manual thresholding segmentation process. A conservative thresholding value was manually chosen that would best consider only the air voids based on the histogram of the before and after healing volumes. An intensity range of 0–17171 (on 16-bit images) was settled on and applied to scans from date 0 and 28 after confirming that both grey-scale histograms did not change. Then, a cylindrical region of interest of 46.25 mm in diameter and 46.35 mm high was selected to remove non-mortar information from the analysis. Morphological attributes were assigned to each element, and the crack system was then isolated from the rest of the pores and air voids using a filter analysis based on the 3D volume values (Fig. 2). Given that the crack can be considered as a single large pore, with a small maximum opening compared to its equivalent diameter and a large total volume, it was easy to filter out as all air voids have a similar maximum opening and equivalent diameter and a smaller total volume. This allowed us to simplify the volume analysis workflow, and only features above the maximum resolution were accounted for. Then, the volume difference was calculated and regarded as the effective crack healing of each sample.

The volume differences only provided a value of the volume change before and after healing. As such, in order to visualize and quantify the healing products, the reconstructed cracks at both ages were subtracted from each other. This yielded a greyscale image that represented the changes during submersion under water for 28 days, i.e. the healing products (Fig. 3C, E). These changes could then be visualized in a 3D volume to observe where the precipitates had formed.

Finally, a slice fraction analysis was performed after acquiring the crack volume subtraction, whereby the fraction occupied by the healing

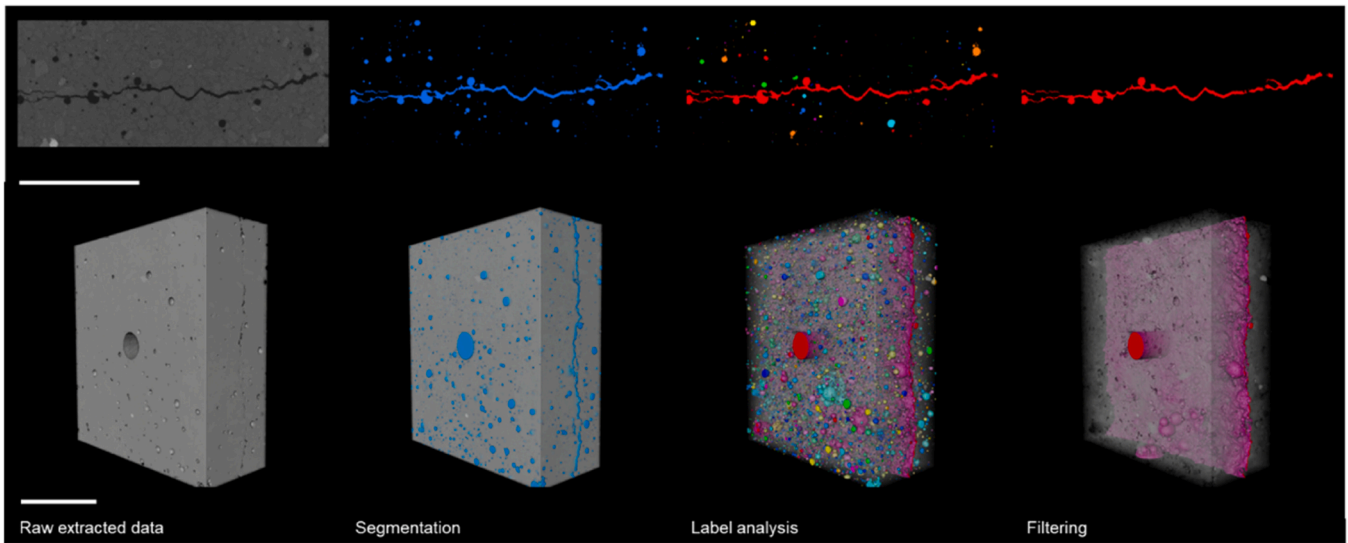


**Fig. 2.** Simplified schematic representation of the image analysis workflow on a step-by-step basis. Top shows a 2D cross section of the 3D volume represented below. From left to right: Raw data was reconstructed and rendered; air voids (including the crack) were segmented by manual thresholding; all air voids were labelled based on their 3D volume; all air voids smaller than the crack volume were filtered out. NB: The whole cylinder was used for the final analysis. Scale bar: 1.5 cm.

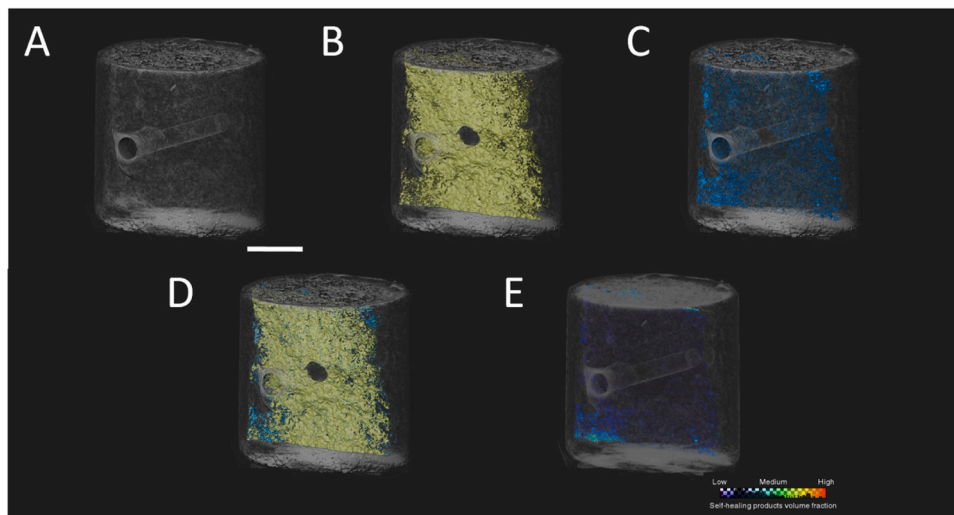


**Fig. 3.** – 3D visualization of the reconstructed volume (A), with the crack volume at date 0 in yellow (B), the resulting healing products at date 28 in blue (C), and overlapped crack volume and healing products (D). Density map of the healing products highlighting the location of the self-healing products by size (E). Scale bar: 1.5 cm.

products in each of the 1873 slices of the total scanned volume was calculated as:

$$Slice\ fraction(\%) = \frac{\sum healing\ products}{Slice\ volume} * 100,$$

where the slice volume is  $56000 \times 56000 \times 30 \mu m$  (length x width x height).

### 2.3. Healing efficiency coefficients

In order to compare the different tests to each other all measurements were converted to healing efficiencies (HE).

The HE of crack widths ( $HE_w$ ) tests was calculated as:

$$HE_w = \frac{Crack\ width\ before\ healing - Crack\ width\ after\ healing}{Crack\ width\ before\ healing} * 100$$

The HE of water flow tests ( $HE_q$ ) was calculated as:

$$HE_q = \frac{Average\ water\ flow\ rate\ before\ healing - Average\ water\ flow\ rate\ after\ healing}{Average\ water\ flow\ rate\ before\ healing} * 100$$

The HE of the crack volume analysis ( $HE_v$ ) was calculated as:

$$HE_v = \frac{\text{Crack volume before healing} - \text{Crack volume after healing}}{\text{Crack volume before healing} - \text{Volume of cast-in-hole}} \times 100$$

The subtraction in the denominator of the last equation was a correction for the cast-in-hole. Due to the cast-in-hole having as big a volume ( $870 \text{ mm}^3$ ) as the crack of most samples, the conversion to HE was skewed as this volume would never heal. For this, the mathematical correction was performed, namely subtracting the cast-in-hole volume from the crack volume, in order to account for this when converting to HE. To corroborate that the mathematical removal of the cast-in-hole was an accurate approximation applicable to all samples, three of the nine samples scanned with micro-CT had further image analysis steps to confirm the approximation accuracy, which can be found in the supplementary data. To compare significant differences of HE between groups a one way ANOVA test ( $p = 0.05$ ) was performed on R.

### 3. Results and discussion

#### 3.1. Sample requirements for coupled test

The main limiting factor in the design of the samples was adjusting the size of the specimen to be representative for all the three tests coupled. Micro-CT scans require small specimens in order to achieve high resolutions. For example, Snoeck et al. [14] used small  $10 \times 6 \text{ mm}^3$  (height x diameter) cylinders to reach a resolution of  $6 \mu\text{m}$  while Kontiza et al. [17] chose prisms of  $20 \times 5 \times 5 \text{ mm}^3$  (length x width x thickness) to reach a voxel size of  $9 \mu\text{m}$ . Such small samples were not possible in this case, given that for water permeability tests, the flow of water that goes through the sample is affected by the crack width [22]. For this, standard sized prisms with crack lengths of  $40 \text{ mm}$  are generally tested. Furthermore, the commonly chosen  $300 \mu\text{m}$  crack width for self-healing tests, which is often beyond what autogenous healing can heal [3], would be non-representative in such small specimens. Finally, small cores are generally obtained through wet drilling or cutting, which is not desirable or not possible for softer binders such as the M33L67 mix tested in this work.

This meant that it was necessary to work with larger sized specimens. Few studies using micro-CT have looked at self-healing in larger samples. Zhang et al. [23] prepared specimens of  $50 \text{ mm}$  in diameter to achieve a resolution of  $56 \mu\text{m}$  voxel size, yet their work was limited to qualitative assessments of the internal healing of the crack. Meanwhile, Van Stappen et al. [15] who were interested in looking at the release of healing agents into the sample, chose a  $60 \times 60 \times 60 \text{ mm}^3$  sample to visualize the capsules embedded in the matrix of the mortars, yet reached a voxel size of  $46.3 \mu\text{m}$ . Nevertheless, the process of healing through polymers is observable at lower magnifications than those of autogenous healing, which meant that lower resolutions were sufficient. Interestingly, Fukuda et al. [20] performed SEM analysis up to a magnification of  $1000\times$  and micro-CT scans with voxel size of  $16 \times 16 \times 25 \mu\text{m}$  (length x width x depth) on the same area of study. Despite the resolution differences reached by both techniques, they showed that there was a good correlation and agreement in terms of self-healing measurements at this resolution.

In the final sample design for this work (Fig. 1), a balance was struck for a sample size of  $45 \text{ mm}$  in diameter, with which a voxel size of  $30 \mu\text{m}$  was achieved, close to the resolution achieved by Fukuda et al. [20] who showed that a  $25 \mu\text{m}$  voxel was good enough in resolution to show the onset of self-healing. This size still allows for a large enough crack mouth for representative microscopy and water permeability tests. Cylinders were chosen to maximize the effectiveness of the detector's surface and to reach the highest resolution possible by closing the distance between the X-ray source and the sample stage. The samples were cast with a rod

to create a cast-in-hole for the adapted water flow tests. A Brazilian splitting test was used to crack the specimen as this allows the creation of a single crack on a localized area of study. Alternatively, it is possible to damage samples through compression, but this can lead to a more complex and variable crack system [24]. Furthermore, compressive loading also creates several microcracks which are known to have a large effect on the 3D volume healing [18]. Having a single crack reduced the variables at the time of study. The maximum width of the crack was adjusted to  $\sim 300 \mu\text{m}$  using a commercial plastic clamp on the cylindrical sample. The use of plastic was necessary as metal which is more often used, would interfere with the X-rays.

#### 3.2. Crack width measurements

The crack width was measured before and after healing to observe the progress of self-healing at the surface of the samples. First, an average crack width of  $\sim 300 \mu\text{m}$  was achieved for all 9 samples at date 0, indicating that the plastic clamps were successful in adjusting the crack width. Nevertheless, a large standard deviation was observed in the crack width (Fig. 4) for each individual sample. This was due to the Brazilian splitting method used to create the cracks which produces V-shaped cracks, which are wider at one end of the crack mouth (Supplementary Figure 1). Despite the shape of the crack mouth, after the healing period all samples showed a reduction in the crack width (Fig. 4). A randomized block design statistical analysis was performed to determine whether healing occurred to different extent depending on the wider or narrower end of the crack. It was possible to isolate the crack location through a block design in the statistical analysis, as the crack width was similar at each location between the samples (Supplementary Figure 2). Naturally, the chosen location along the crack length (at the mouth) had an effect on the healing efficiency due to the varying width ( $100 - 300 \mu\text{m}$ ), with the wider sections across all formulations showing very little healing. Still, the cracks were significantly different before and after healing for all samples for  $p < 0.05$ .

The importance of crack width in the healing efficiency as demonstrated by the varying crack size of the samples, stresses the limitations of previous micro-CT studies performed with smaller specimens. While smaller cracks may have shown good healing, their results may not be representative of the results obtained with other techniques that assess larger and more typical crack sizes. As such, these studies may not offer a complete representation of the self-healing capacity of the studied materials, despite their precision in depicting outcomes in smaller samples.

Of the formulations tested, C100L0 had the best healing efficiency of cracks ( $HE_w$ ) on average while M33L67 was the least effective. Regardless, the formulation had non-significant effect on the healing efficiency.

#### 3.3. Change in water flow

Like the crack width measurements, the water flow test showed a significant reduction in flow for all samples ( $p < 0.05$ ), indicating that the self-healing products were sound (Fig. 5). Still, the extent of autogenous healing was rather limited. Analysis of the healing efficiency ( $HE_q$ ) between formulations showed that M33L67 had a tendency to underperform in comparison with C50L50 and C100L0, despite that these differences were not significant ( $p < 0.05$ ). This can be attributed to the differences in the self-healing products expected to have been formed. Considering that the samples were cracked at 7 days, the hydration reactions were still ongoing, while the fact that the samples were taken from 95 % RH to be submerged under water highly reduced the formation of carbonation products. This likely promoted the formation of hydration products in the cracks of cement containing formulations and pozzolanic reactions in the lime-metakaolin binder mix. The cement hydration proceeds faster than the pozzolanic reactions, explaining the better performance of the cement-containing mixtures [25]. Although, it was expected for precipitation of carbonation products in the

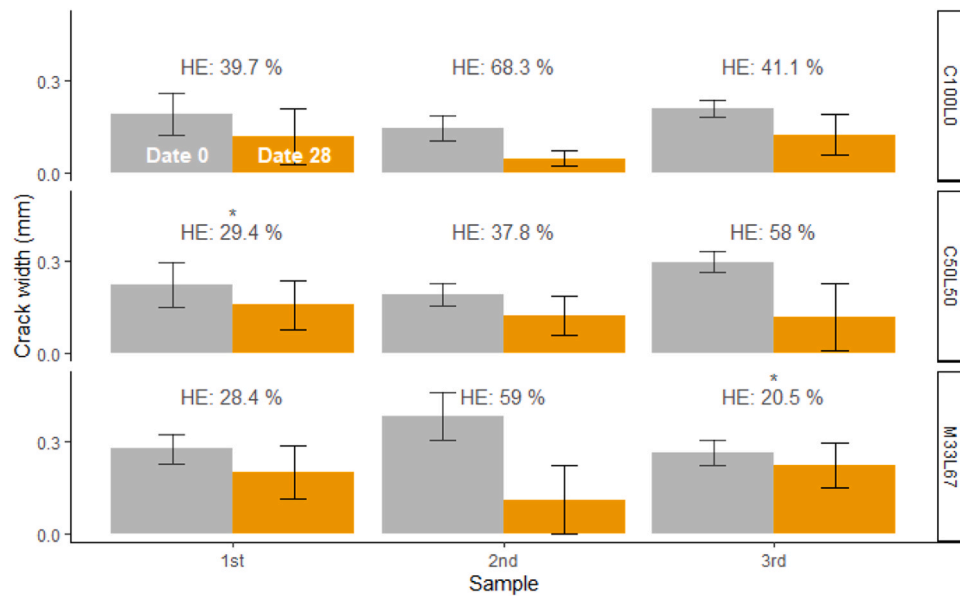


Fig. 4. – Average crack width for each sample of all three formulations at date 0 (grey bars) and date 28 (yellow bars) after healing, with indication of the calculated HE<sub>w</sub>. Three ROIs per sample were measured to calculate the average crack width and the standard error (error bars). \* indicates non-significant healing for  $p < 0.05$ .

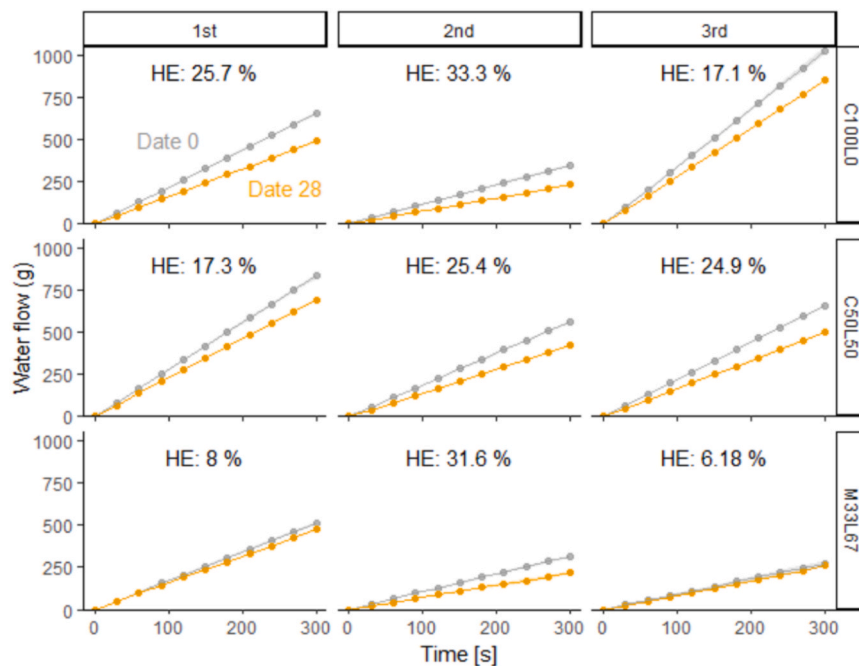
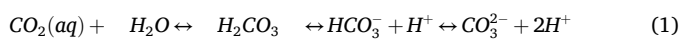


Fig. 5. – Water flow values obtained at date 0 (grey lines) and date 28 (yellow lines) after healing on all three formulations, with indication of the calculated HE<sub>q</sub>. Measurements were performed in triplicates with a low percentage of variability.

lime-containing mixtures to be low, any formation would have likely happened through diffusion of CO<sub>2</sub> dissolved in the water (Eq.1) and reaction with free Ca<sup>2+</sup> from dissolved Ca(OH)<sub>2</sub> (Eqs.2–3) [26]. The fact that diffusion occurred through water and not air would have made this process 10000 times slower, though [27]. Such a difference in diffusion rates is seen as a barrier to CO<sub>2</sub> transfer to the reaction front in water-saturated pores, leading to a reduced formation of carbonation self-healing products [27].



Besides the lower performance, M33L67 also had the most variation in HE<sub>q</sub>. This variation might arise from M67L33 samples' inherent lower tensile strength which can cause more tortuous and inconsistent cracks when cracking. Previously, Edvardsen [26] proposed equation (Eq.4) to model water flow ( $q$ ) through a natural crack, and defined a reduction factor to adjust for the roughness of naturally occurring cracks ( $\xi$ ):

$$q = \frac{\xi \cdot \Delta p \cdot b \cdot w^3}{12\eta \cdot d} \quad (4)$$

where  $\Delta p$  is the differential water pressure between inlet and outlet of a

crack (in  $N/m^2$ ),  $w$  is the width of the crack (in m),  $\eta$  the absolute viscosity of the fluid passing through the crack (in  $Ns/m^2$ ) and  $d$  is the thickness of the structure through which the water flows (in m). Following the same reasoning Van Mullem et al. [22] applied to simplify the relation between  $q$  and  $w$ , it is possible to relate  $q$  to crack geometry, by rewriting Eq. 4 as:

$$q = \xi \bullet A \tag{5}$$

where  $A$  is a constant, given that the setup used was the same for all samples, the samples had the same dimensions and an average crack width was similar for all samples.

It is important to highlight that the water flow of the adapted samples showed an acceptably low variability (COV 0.01–0.04) between the three repetitions on the same samples before healing – a requirement by Van Mullem et al. [22] to ensure that the test was consistent and repeatable. This showed that it was possible to implement water flow tests in these adapted samples for micro-CT.

Overall, C100L0 showed the best  $HE_w$  and  $HE_q$  while M33L67 was the least effective, even though these differences were non-significant. In fact, there was a clear correlation between high  $HE_w$  and  $HE_q$  in all samples ( $r = 0.88$ ) (Fig. 6), which has been previously established with other water permeability tests and in concrete [27]. Despite the positive correlation between  $HE_w$  and  $HE_q$ , the magnitude of  $HE_w$  was larger than  $HE_q$ . The difference in magnitude was also seen in the work of Roig-Flores et al. [27] although not expanded upon. This difference could be explained due to the nature of the tests. Whereas microscopy measurements were limited to the three ROIs at the crack surface, water flow tests measure a phenomenon across length and height of the whole crack, encompassing surface and internal aspects as well as durability of the healing products. As such, unmeasured changes in the crack mouth could still have an impact on water flow tests. For example, it is possible that for the 2nd and 3rd C50L50 samples, with the same  $HE_q$  but different  $HE_w$  (Table 4), healing occurred to the same extent in the samples but the specific ROIs chosen for crack width measurements or the depth of the formation of the products in each sample showed varying degree of healing.

The inability to firmly determine the cause of sample variability, likely due to whether the healing within the sample was as extensive as on the surface, illustrates that self-healing is a phenomenon influenced by multiple parameters that need to be measured in 3D to be able to fully characterize the system, as stated by Van Stappen et al. [15]. Therefore, the use of micro-CT offers a valuable insight into understanding how internal changes in the crack system lead to differences between changes

**Table 4 –**

Summary table showing HE values (%) for all three tests on studied samples alongside average and standard deviation per formulation.

Formulation	Sample	$HE_w$	$HE_q$	$HE_v$
C100L0	1st <sup>a</sup>	40	26	3.7
	2nd	68	33	16
	3rd	41	17	2.6
	Average	50	25	7
	St. dev.	13	7	6
C50L50	1st	29	17	8.4
	2nd <sup>a</sup>	38	25	10
	3rd	58	25	1
	Average	42	22	6
	St. dev.	12	4	4
M33L67	1st <sup>a</sup>	28	8	24
	2nd	59	32	2.2
	3rd	20	6	4.6
	Average	36	15	10
	St. dev.	17	12	10

<sup>a</sup> indicate samples analyzed in-depth using image analysis software.

in the crack width and water flow tests.

### 3.4. Crack volume analysis using micro-CT

The crack volume at date 0 and date 28 was extracted through volume analysis of the micro-CT scans and the progression of healing in the crack was calculated from the change in volume. Similarly to the two previous tests, no significant difference was observed for  $HE_v$  between formulations ( $p < 0.05$ ). This time, no trend was present between formulations, either. All samples had a lower crack volume after the healing cycle, but the magnitude of the decrease differed, leading to a different  $HE_v$ , with two samples as outliers, namely the 3rd M33L67 sample which showed a 24 % decrease and the 2nd C100L0 sample which reduced by 16 % (Table 4). The rest of the samples showed limited healing.

During the initial stages of the volume analysis two thresholding values, one more conservative (intensity range 0–17171) than the other (0–20190), were used to perform crack volume calculations based on the greyscale distribution in the histogram together with visual observations. Multiple thresholds were chosen to explore which values returned the most reliable results. The lower threshold value was selected for the image analysis of healing products, as they returned more conservative values and prevented overestimation of quantitative measurements. This reduced the chances of highly skewed results due to errors, such as considering the lighter greyscales allocated to the binder as part of the crack system along the edges.

The  $HE_v$  of the crack volume as obtained by micro-CT shows no correlation with  $HE_w$  ( $R = 0.02$ ) (Fig. 6) or  $HE_q$  ( $R = 0.05$ ) (correlation between  $HE_v$  and  $HE_q$  in Supplementary Figure 3). This highlights the considerable variability of internal crack healing of mortars. Furthermore, it indicates that healing is happening at the crack opening, which is studied by microscopy and water flow tests, but it does not fully represent the true healing occurring through the sample. As such, using limited testing methods might not provide a robust understanding of the true effectiveness of self-healing agents or formulations when studied in isolation. To our knowledge, the use of coupled techniques is a relatively uncommon approach in the study of self-healing. One example of such work is from Fan and Li [18], who reported the relationship between micro-CT volume differences with other tests using the same samples. It was observed that resonance frequency and microscopy tests did not show good agreement with crack volume changes. On the other hand, stiffness recovery showed almost direct association to crack volume changes. These results are consistent with those reported by Sidiq et al. [16] who saw a correlation between  $HE_v$  and compressive strength but not  $HE_w$ , although they performed each test on a different series of samples. It should be stressed, even though crack width measurements

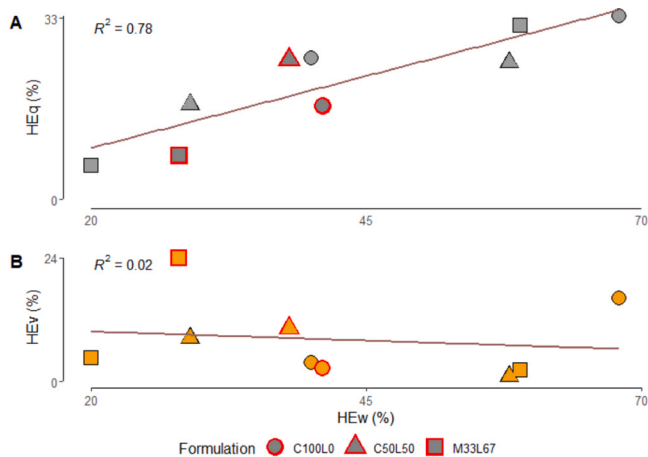


**Fig. 6. –** Correlation of  $HE_q$  vs  $HE_w$  (A) and  $HE_v$  vs  $HE_w$  (B) with a linear regression model and the respective  $R^2$  values. The red outlines indicate the samples analyzed in-depth using image analysis software. Correlation between  $HE_v$  and  $HE_q$  can be seen in Supplementary Figure 3.

are the go-to technique for quantifying self-healing in most cases, they do not seem to provide a robust evaluation that is representative for the entire crack system [2]. As such, we present a contribution towards the application of more robust and comprehensive testing towards understanding self-healing in construction mortars.

### 3.5. Self-healing products analysis using micro-CT

To further understand the internal changes occurring in the specimens, three of them were analyzed in depth by image analysis. This was limited to one specimen per formulation due to the time-consuming and resource-intensive nature of image analysis. Given that the samples were designed to be closer in size to standard specimens more often used in other studies, it is expected that the dynamics observed in the selected samples would be representative of self-healing, despite the expected heterogeneities that occur from sample to sample of a similar mixture. Crack width change, the most commonly measured parameter in self-healing, was taken as a reference for comparison between formulations. As such, three samples with similar  $HE_W$  from each formulation were studied further. The three selected samples (Table 4) covered the whole spectrum of the tested variables: the 2nd M33L67 sample showed large  $HE_V$  and low  $HE_q$ , the 3rd C100L0 sample showed moderate  $HE_q$  and low  $HE_V$  and the 2nd C50L50 sample had a higher  $HE_q$  and an intermediate  $HE_V$  (Fig. 6).

For each sample, the self-healing products or precipitates were isolated through the differential volume obtained by the subtraction of the reconstructed crack volumes before and after healing. The fraction occupied by all healing products per slice of the reconstructed volumes was calculated using image analysis software (Avizo 2020.3). The analysis of the sizes of the slice fractions shows that the extent of healing in each sample was widely distributed (Fig. 7). The lime-containing formulations had a bimodal size distribution of healing, with M33L67 having overall regions with less healing products than C50L50. C50L50 also had a more rightwards skew towards regions with more healing than the other formulations. C100L0 had a normal distribution. Interestingly, the number of non-zero slice fractions was similar. This meant that major volume differences can be attributed to the overall size of the healing products at specific locations.

The slice fraction was also used to identify the areas along the height of the crack where healing was most predominant (Fig. 8). In M33L67 healing products were located at the top of the crack but not directly at the mouth. Meanwhile, in C50L50, these were at the top, specifically at the mouth, and bottom, i.e. also at the sealed side of the crack. The presence of healing products at the top of the crack is likely due to the

requirement of  $CO_2$  and moisture ingress for the formation of precipitated healing products, and as these diffuse into the crack, they will first react with the unreacted material at the crack opening [28]. This has been extensively reported previously [18,20,23,29]. With regards to the rest of the crack, healing was consistent over its depth in all formulations. This has been reported for cracks of sufficient width ( $> 100 \mu m$ ), which allow faster transport of water allowing the formation of healing products deeper in the crack, mainly continued hydration of cement and pozzolanic reactions from metakaolin [18]. Overall, the concentration of healing products at the crack mouth also explains how reductions in water flow and crack width changes were reported and did not correlate to the overall volume decrease measured in the cracks of some samples.

On a side note, it is important to highlight that aforementioned works often do not reported how the samples were placed during healing, and it is not possible to know whether the formation of healing products is influenced by the positioning of the samples, or if it spontaneously occurs in this way. In this work, the samples were placed with the crack mouth facing downwards, and only M33L67 showed preference for the formation of healing products at the crack mouth. Therefore, the effect of positioning of samples during healing remains a debated topic and the positioning should be reported in the literature in order to reach more certain conclusions [30].

The slice fractions presented above only provide a 2D representation along the height of the crack of what was measured in 3D. Visualizing the healing in 3D (Fig. 9) shows more accurately clusters of healing products rather than an even distribution along the length and height of the crack. This is clear for the C50L50 sample where there is a clustering of healing products at the bottom edges of the cylinder (Fig. 9). The healing at the top surface seemed better distributed along the length of the crack. On the other hand, C100L0 showed a more evenly distributed healing progress, as seen on the slice fraction analysis.

Moreover, the influence of pores on the healing became apparent upon 3D analysis of the samples. Particularly, for M33L67 and C100L0 clusters of healing were observed in the bottom half of the samples (Fig. 9). These were pores removed from the crack network due to the precipitation of self-healing products at the pore-crack interface. Fig. 10 shows a slice of the crack volume studied where a pore (top green arrow) is observed in the crack system before (Fig. 10A) and after self-healing (Fig. 10B). The area of the crack before healing (Fig. 10C, green plus white selection) includes this pore, whereas it is observed that the pore is no longer considered in the volume of the crack after healing (Fig. 10C, green selection). This is due to self-healing products precipitating at the pore-crack interface connecting the isolated air void with the rest of the crack network. Areas where self-healing took place (blue arrows) are seen as light grey in the image compared to the darker areas without self-healing (green arrows) such as the pore itself (Fig. 10B). Consequently, the crack system reduced in volume to a greater extent than the volume of the newly formed precipitates.

The change in crack volume has been used as a parameter to assess self-healing before [18]. Yet, the phenomena of pores being blocked off by precipitation of self-healing products at the pore-crack interface can cause a skew on the results on effective self-healing as the measured volume change of the crack appeared to be larger than the actual precipitation of healing products. Interestingly, the influence of pores has not been discussed in previous micro-CT studies even though micro-CT is an effective tool for such work. Furthermore, this removal of pores could further influence the lack of correlation found between  $HE_W$  and  $HE_V$ . A reduction in pores connected to the crack will have an impact on the crack geometry, which has a strong influence on water permeability tests [22]. For example, it might lead to more water flow as the crack becomes less tortuous and the water achieves more laminar flow. As such, porosity could play an important undescribed effect on self-healing dynamics, particularly in water permeability tests and needs to be further studied.

The influence of pore blocking on the final volumes used to calculate the  $HE_V$  raises the question on how other dynamics can play a role when

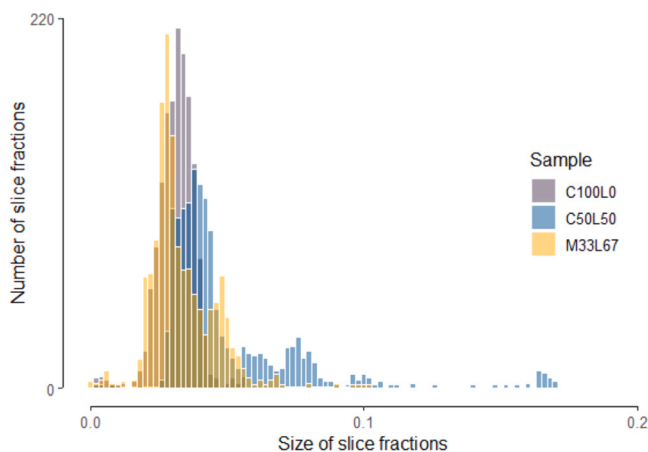
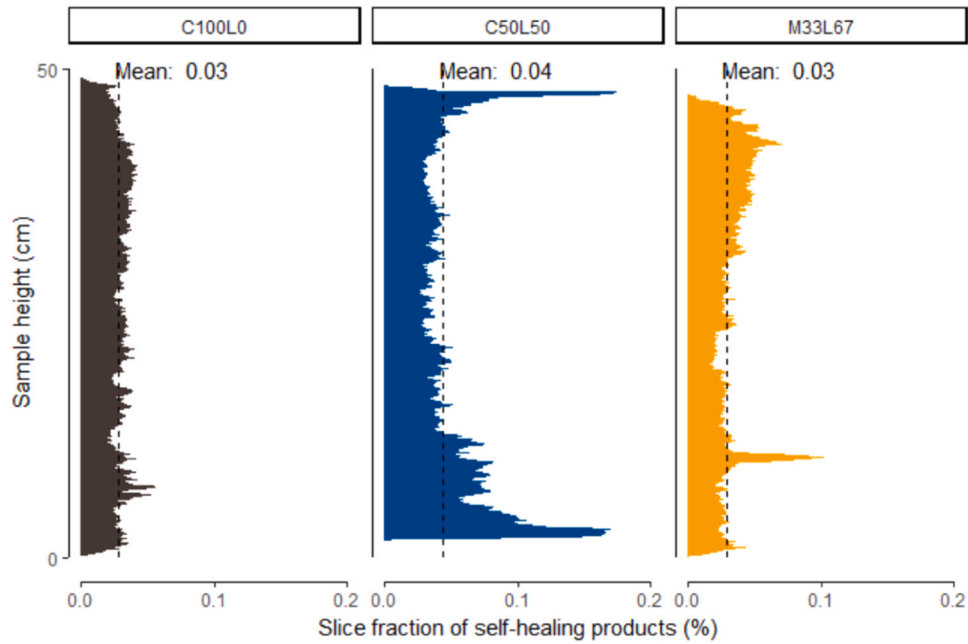
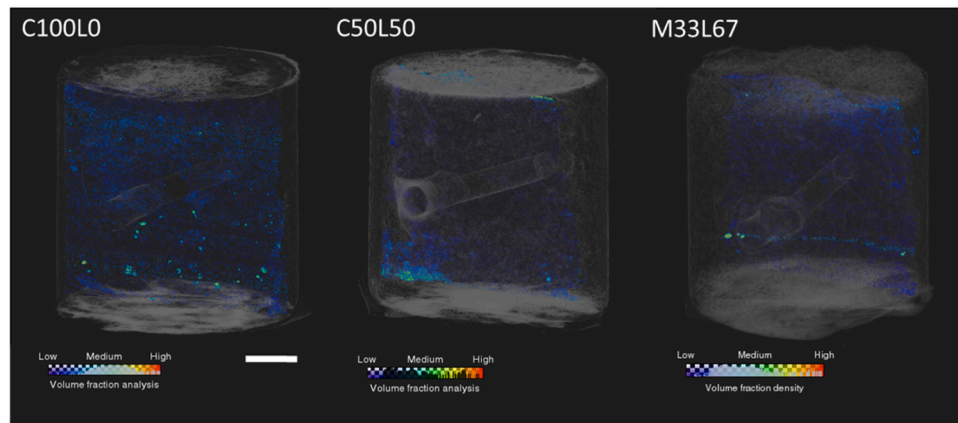


Fig. 7. – Histogram (bin width 0.002) for the slice fractions larger than 0 of a representative sample per formulation. The slice fraction represents the percentage of healing products that occupy a single  $30 \mu m$  slice of the reconstructed volume, with slices taken perpendicular to the cylinder axis.



**Fig. 8.** – Slice fraction analysis of a sample per formulation. The slice fraction represents the percentage of healing products that occupy a single 30 μm slice of the reconstructed volume, with slices taken perpendicular to the cylinder axis. The mean fraction of healing products for each sample is represented by the dotted line.



**Fig. 9.** – Distribution of healing products through the whole crack. Clusters of healing are more visible as indicated by the heat map with red indicating where the larger healing products are and blue the smallest. Scale bar: 1 cm.

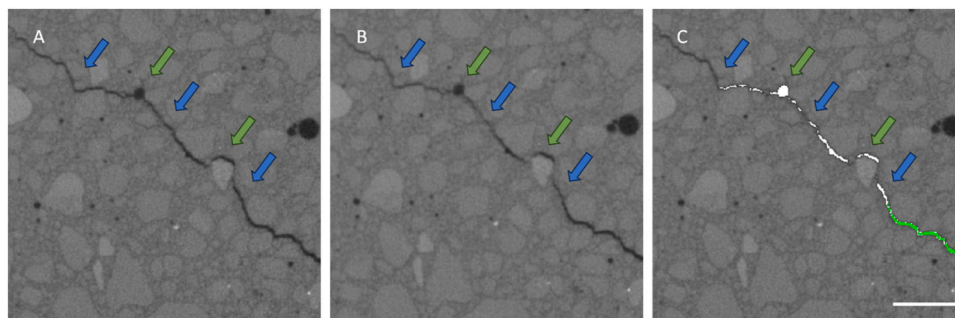


**Fig. 10.** 2D slice of a cracked mortar showing a pore (top green arrow) connected to the crack network before self-healing (A) and after self-healing (B). The healed area (C, white selection) considers both areas of precipitation (blue arrows) and no precipitation (green arrows), due to precipitation happening at the interface between the pore and the rest of the crack. Note that self-healing products are observed in B, as the crack has a different grey value or lower attenuation coefficient than in A, the unhealed crack. Scale bar: 2 mm.

quantifying self-healing in micro-CT. Self-healing occurs by either the reaction of unreacted binder particles or through the dissolution and reprecipitation of reacted hydration and carbonation products. These dissolved products can reprecipitate in the crack or even leach from the mortar matrix in the presence of water, leading to volume differences that cannot be attributed to healing products. Although areas where the crack widened were visible in the scans, it is hard to attribute this process to a specific phenomenon such as particle detachment or dissolution, especially when it is not happening widely in the sample. Certain verifications can be made to confirm this, for example, Schröer [31] confirmed dissolution was occurring in their samples because black regions (indicating deduction) in the subtracted images were visible on both sides of the crack. In our case, the opposite phenomenon occurs, where white regions were observed on both sides of the crack, and therefore, it was possible to assign these changes to precipitation of healing products (Fig. 11).

Furthermore, there is the possibility of detachment of mortar fractions from the crack wall, which can either lead to expansion of the crack as well as mechanically blocking and healing of the crack [32]. Given that all samples were handled in a similar manner this factor should be averaged out. Still, the different binder strengths could mean that lower strength binders will undergo more influence of this phenomenon. Only the movement of large particles in the crack were obvious in this work (Fig. 11).

#### 4. Conclusion

This work showed the importance of how coupled techniques are needed to better explain the phenomenon of self-healing, demonstrated here in lime-based mortars. We aimed at coupling three testing techniques: microscopic crack width measurements to study the progress of self-healing at the crack mouth, water flow tests for the assessment of durability of the self-healing products and micro-CT to understand the relation of the former two techniques to changes in the 3D volume of the crack in a non-destructive manner. The research highlights that microscopy and water permeability tests are not representing in a correct manner the effect of self-healing of an entire crack system. Healing was observed for all samples, albeit the autogenous healing was limited and no significant difference was observed between formulations. No correlation of  $HE_V$  was observed to  $HE_W$  or  $HE_q$ , highlighting that the

results from  $HE_W$  and  $HE_q$  don't fully describe what is happening within the crack. This has not been reported before for water permeability tests and arose from healing occurring predominantly at the mouth of the crack. On the other hand, the  $HE_q$  was correlated to  $HE_W$ , although the magnitude of the two variables was different. Higher  $HE_W$  were observed than for  $HE_q$ , likely due to the microscopic evaluation being focused to certain regions of interest on the crack mouth while water flow tests quantify self-healing along the length and depth of the crack. Such a bias highlights the need of multiple testing techniques used simultaneously to more accurately describe the process of healing, while future research into self-healing should focus on validating these coupled techniques for other autonomous healing technologies. The choice of three different mortar compositions allowed to test the coupled techniques on materials with varying strength. Given that most research on self-healing is performed on cement-based materials, not all techniques are adaptable to all types of mortars (especially low strength mortars) [33].

Furthermore, studies of coupled techniques that assess two or more parameters in the same crack system are limited and should become normalized as they are more robust, save time and numbers of samples. Micro-CT offers an excellent opportunity to couple varying quantitative and descriptive techniques to changes occurring throughout the crack system as shown here. The tortuosity of the crack seemed to have an effect on the  $HE_q$ , with M33L67 being particularly affected by this given its lower strength. Another potential influence on the tortuosity of the crack observed thanks to micro-CT scans, is related to the pores connected to the crack. Qualitative analysis showed that pores were observed to have healed in the volume analysis. Yet, it was shown that the pores did not show self-healing but had been removed from the crack network through precipitation of healing products at the pore-crack interface. This meant the measured volume change of the crack appeared to be larger than the actual precipitation of healing products. Such a phenomenon has not been described previously. This can have an impact on the tortuosity of the crack and as such affect water permeability tests as well. Nevertheless, more research is needed combining both techniques.

At the same time, we worked towards a more representative study of self-healing by using samples that were closer to standard-sizes, given most micro-CT research has focused on achieving high resolution and has thus been applied on very small samples. In technical terms, micro-

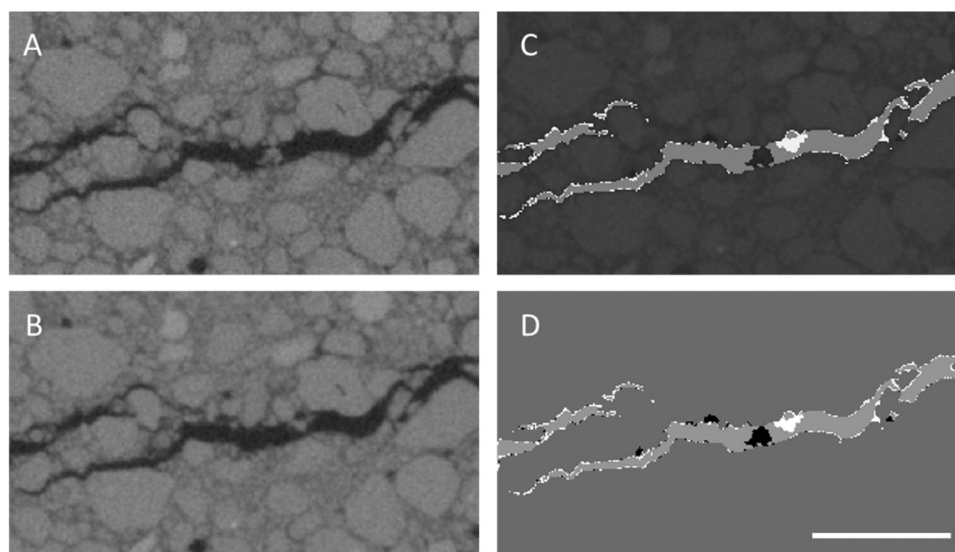


**Fig. 11.** – Dissolution and precipitation processes and shifting of particles visualized through micro-CT in a M33L67 sample. Changes in the crack geometry are observed before (A) and after (B) the healing period. The subtracted images (C-D) show in white those areas that appear in the crack after the healing period and in black those that disappear. White regions in C-D outlining the crack are a strong indication of precipitation while the shifting of a large particle is observed in black in the middle of the crack. Scale bar: 2 mm.

CT faces research constraints when changes are happening beyond the resolution capacity of the scanners, which is limited by the minimum representative size of the tested specimens. In this research, a compromise was made regarding a sample size that would provide sufficient resolution for micro-CT and still allow to obtain representative results for the other measurements by selecting standard-size specimens. The importance of larger samples was highlighted with the observations made on smaller sections of the crack which always saw healing, while wider regions did not. As such the use of small samples might not be showing representative healing efficiencies of the studied materials as more healing would be expected due to the smaller crack sizes. Nevertheless, for micro-CT studies it is often argued that small samples are needed to achieve good resolutions, yet here it was shown how larger samples are possible without compromising on the resolution needed to measure self-healing with micro-CT. The resolution may be insufficient to visualize precisely what is happening only if studying micro-cracks. As such, the authors recommend to use even larger samples that are more representative in future studies.

Nonetheless, micro-CT is not without flaws. Its computational demands and time-consuming analysis can be challenging, while its learning curve is steep for initiating users. Furthermore, as the analysis process involves the use of image analysis software, the workflow becomes user-dependent, for instance, on the choice of a particular segmentation threshold which was a consideration made in this work. Although certain quality checks can be performed, such as choosing more conservative thresholding values, it is necessary to keep the operator bias in mind.

Lastly, to our knowledge, this is the first time that self-healing in lime-based mortars is reported for the whole crack and that the use of micro-CT is reported for such formulations. Overall, work in lime-based binders remains very limited, although there has been a recent rise in interest in alternatives to cement-containing mortars. Nevertheless, many research techniques in the area of self-healing have been developed for cement mortars which have higher strength and are not adapted for low-strength binders [33], such as the M33L67 used in this work. This work also shows the potential of micro-CT as a feasible technique to study self-healing in these materials.

#### CRediT authorship contribution statement

**Nele De Belie:** Writing – review & editing, Supervision, Funding acquisition. **Nico Boon:** Funding acquisition. **Veerle Cnudde:** Writing – review & editing, Supervision. **Franco Grosso Giordano:** Software, Methodology, Investigation, Formal analysis, Data curation, Conceptualization. **Dulce Valdez Madrid:** Software, Methodology, Data curation. **Laurenz Schröer:** Investigation.

#### Declaration of Competing Interest

The authors declare the following financial interests/personal relationships which may be considered as potential competing interests: Franco Grosso Giordano reports financial support was provided by EU Framework Programme for Research and Innovation Marie Skłodowska-Curie Actions. Franco Grosso Giordano reports financial support was provided by EU Framework Programme for Research and Innovation Research Infrastructures and E-Infrastructures. If there are other authors, they declare that they have no known competing financial interests or personal relationships that could have appeared to influence the work reported in this paper.

#### Data availability

Micro-CT data will be uploaded to YODA repository of Utrecht University at <https://public.yoda.uu.nl/geo/UU01/MSBPLS.html>. All other data available upon request.

#### Acknowledgements

This research has been carried out within the framework of the EU SUBLime network. This Project has received funding from the European Union's Horizon 2020 research and innovation programme under Marie Skłodowska-Curie project SUBLime [Grant Agreement n°955986]. Furthermore, the authors also want to acknowledge funding for the micro-CT scans and software access from the European Union's Horizon 2020 research and innovation programme under grant agreement n°101005611 for Transnational Access conducted at the Centre for X-ray Tomography of Ghent University (UGCT) (BOF.COR.2022.0009). We thank Vadim Grigorjev for providing the particle size distribution of the materials used.

#### Appendix A. Supporting information

Supplementary data associated with this article can be found in the online version at [doi:10.1016/j.conbuildmat.2024.136603](https://doi.org/10.1016/j.conbuildmat.2024.136603).

#### References

- [1] A.I. Omeregic, K. Muda, O.O. Ojuri, C.Y. Hong, F.M. Pauzi, N.S.B.A. Ali, The global research trend on microbially induced carbonate precipitation during 2001–2021: a bibliometric review, *Environ. Sci. Pollut. Res.* 29 (2022) 89899–89922, <https://doi.org/10.1007/s11356-022-24046-w>.
- [2] V. Cappellesso, D. di Summa, P. Pourhaji, N.P. Kannikachalam, K. Dabral, L. Ferrara, M. Cruz Alonso, E. Camacho, E. Gruyaert, N. De Belie, A review of the efficiency of self-healing concrete technologies for durable and sustainable concrete under realistic conditions, *Int. Mater. Rev.* 68 (2023) 556–603, <https://doi.org/10.1080/09506608.2022.2145747>.
- [3] N. De Belie, E. Gruyaert, A. Al-Tabbaa, P. Antonaci, C. Baera, D. Bajare, A. Darquennes, R. Davies, L. Ferrara, T. Jefferson, C. Litina, B. Miljevic, A. Otlewska, J. Ranogajec, M. Roig-Flores, K. Paine, P. Lukowski, P. Serna, J. M. Tulliani, S. Vucetic, J. Wang, H.M. Jonkers, A review of self-healing concrete for damage management of structures, *Adv. Mater. Interfaces* 5 (2018) 1800074, <https://doi.org/10.1002/ADMI.201800074>.
- [4] Y.S. Lee, W. Park, Current challenges and future directions for bacterial self-healing concrete, *Appl. Microbiol. Biotechnol.* 102 (2018) 3059–3070, <https://doi.org/10.1007/s00253-018-8830-y>.
- [5] B. Liu, M. Wu, W. Du, L. Jiang, H. Li, L. Wang, J. Li, D. Zuo, Q. Ding, The application of self-healing microcapsule technology in the field of cement-based materials: a review and prospect, *Polym.* 15 (2023) 2718, <https://doi.org/10.3390/polym15122718>.
- [6] A. Ravitheja, T. Chandra Sekhara Reddy, C. Sashidhar, Self-healing concrete with crystalline admixture - a review, 11430–1154, *J. Wuhan. Univ. Technol. Sci. Ed.* 34 (2019), <https://doi.org/10.1088/1757-899X/660/1/012057>.
- [7] A. Mignon, N. De Belie, P. Dubruel, S. Van Vlierberghe, Superabsorbent polymers: a review on the characteristics and applications of synthetic, polysaccharide-based, semi-synthetic and 'smart' derivatives, *Eur. Polym. J.* 117 (2019) 165–178, <https://doi.org/10.1016/j.eurpolymj.2019.04.054>.
- [8] A. Al-Fakih, M.A.A. Mahamood, M.A. Al-Osta, S. Ahmad, Performance and efficiency of self-healing geopolymer technologies: a review, *Constr. Build. Mater.* 386 (2023) 131571, <https://doi.org/10.1016/j.conbuildmat.2023.131571>.
- [9] F. Grosso Giordano, N. Boon, N. De Belie, Influence of Hydrated Lime on the Self-healing capacity of cement mortars, *MATEC Web Conf.* 378 (2023) 02021, <https://doi.org/10.1051/mateconf/202337802021>.
- [10] C. De Nardi, A. Cecchi, L. Ferrara, A. Benedetti, D. Cristofori, Effect of age and level of damage on the autogenous healing of lime mortars, *Compos. Part B Eng.* 124 (2017) 144–157, <https://doi.org/10.1016/j.compositesb.2017.05.041>.
- [11] R. Jakubovskis, A. Jankutė, J. Urbonavičius, V. Grišniak, Analysis of mechanical performance and durability of self-healing biological concrete, *Constr. Build. Mater.* 260 (2020) 119822, <https://doi.org/10.1016/J.CONBUILDMAT.2020.119822>.
- [12] V. Cnudde, M.N. Boone, High-resolution X-ray computed tomography in geosciences: a review of the current technology and applications, *Earth Sci. Rev.* 123 (2013) 1–17, <https://doi.org/10.1016/j.earscirev.2013.04.003>.
- [13] P.J. Withers, C. Bouman, S. Carmignato, V. Cnudde, D. Grimaldi, C.K. Hagen, E. Maire, M. Manley, A. Du Plessis, S.R. Stock, X-ray computed tomography, *Nat. Rev. Methods Prim.* 1 (2021) 18, <https://doi.org/10.1038/s43586-021-00015-4>.
- [14] D. Snoeck, J. Dewanckele, V. Cnudde, N. De Belie, X-ray computed microtomography to study autogenous healing of cementitious materials promoted by superabsorbent polymers, *Cem. Concr. Compos.* 65 (2016) 83–93, <https://doi.org/10.1016/j.cemconcomp.2015.10.016>.
- [15] J. Van Stappen, T. Bultreys, F.A. Gilbert, X.K.D. Hillewaere, D.G. Gómez, K. Van Tittelboom, J. Dhaene, N. De Belie, W. Van Paepegem, F.E. Du Prez, V. Cnudde, The microstructure of capsule containing self-healing materials: a micro-computed tomography study, *Mater. Charact.* 119 (2016) 99–109, <https://doi.org/10.1016/j.matchar.2016.07.014>.

- [16] A. Sidiq, R.J. Gravina, S. Setunge, F. Giustozzi, Microstructural analysis of healing efficiency in highly durable concrete, *Constr. Build. Mater.* 215 (2019) 969–983, <https://doi.org/10.1016/j.conbuildmat.2019.04.233>.
- [17] A. Kontiza, D. Semitekolos, T.K. Milickovic, P. Pappas, N. Koutroumanis, C. Galiotis, C.A. Charitidis, Double cantilever beam test and micro-computed tomography as evaluation tools for self-healing of CFRPs loaded with DCPD microcapsules, *Compos. Struct.* 279 (2022) 114780, <https://doi.org/10.1016/j.comstruct.2021.114780>.
- [18] S. Fan, M. Li, X-ray computed microtomography of three-dimensional microcracks and self-healing in engineered cementitious composites, *Smart Mater. Struct.* 24 (2015) 015021, <https://doi.org/10.1088/0964-1726/24/1/015021>.
- [19] J. Wang, J. Dewanckele, V. Cnudde, S. Van Vlierberghe, W. Verstraete, N. De Belie, X-ray computed tomography proof of bacterial-based self-healing in concrete, *Cem. Concr. Compos.* 53 (2014) 289–304, <https://doi.org/10.1016/j.cemconcomp.2014.07.014>.
- [20] D. Fukuda, M. Maruyama, Y. Nara, D. Hayashi, H. Ogawa, K. Kaneko, Observation of fracture sealing in high-strength and ultra-low-permeability concrete by micro-focus X-ray CT and SEM/EDX, *Int. J. Fract.* 188 (2014) 159–171, <https://doi.org/10.1007/s10704-014-9952-6>.
- [21] T. Van Mullem, G. Anglani, M. Dudek, H. Vanoutrive, G. Bumanis, C. Litina, A. Kwiecień, A. Al-Tabbaa, D. Bajare, T. Stryzewska, R. Caspee, K. Van Tittelboom, T. Jean-Marc, E. Gruyaert, P. Antonaci, N. De Belie, Addressing the need for standardization of test methods for self-healing concrete: an inter-laboratory study on concrete with macrocapsules, *Sci. Technol. Adv. Mater.* 21 (2020) 661–682, <https://doi.org/10.1080/14686996.2020.1814117>.
- [22] T. Van Mullem, E. Gruyaert, B. Debbaut, R. Caspee, N. De Belie, Novel active crack width control technique to reduce the variation on water permeability results for self-healing concrete, *Constr. Build. Mater.* 203 (2019) 541–551, <https://doi.org/10.1016/j.conbuildmat.2019.01.105>.
- [23] L.V. Zhang, A.R. Suleiman, M.L. Nehdi, Self-healing in fiber-reinforced alkali-activated slag composites incorporating different additives, *Constr. Build. Mater.* 262 (2020) 120059, <https://doi.org/10.1016/j.conbuildmat.2020.120059>.
- [24] A. Sidiq, R.J. Gravina, S. Setunge, F. Giustozzi, High-efficiency techniques and micro-structural parameters to evaluate concrete self-healing using X-ray tomography and Mercury Intrusion Porosimetry: a review, *Constr. Build. Mater.* 252 (2020) 119030, <https://doi.org/10.1016/j.conbuildmat.2020.119030>.
- [25] Ö. Cizer, K. Van Balen, D. Van Gemert, Competition between hydration and carbonation in hydraulic lime and lime-pozzolana mortars, 241–246, *Adv. Mater. Res.* (2010) 133–134, <https://doi.org/10.4028/www.scientific.net/AMR.133-134.241>.
- [26] C. Edvardsen, Water permeability and autogenous healing of cracks in concrete, *Acids Mater. J.* 96 (1999) 448–454, <https://doi.org/10.1680/iicsdac.28241.0047>.
- [27] M. Roig-Flores, S. Moscato, P. Serna, L. Ferrara, Self-healing capability of concrete with crystalline admixtures in different environments, *Constr. Build. Mater.* 86 (2015) 1–11, <https://doi.org/10.1016/j.conbuildmat.2015.03.091>.
- [28] H.M. Jonkers, E. Schlangen, Development of a bacteria-based self healing concrete, *Taylor Made Concr. Struct.* 1 (2008) 425–430, <https://doi.org/10.1201/9781439828410.ch72>.
- [29] G. Fang, Y. Liu, S. Qin, W. Ding, J. Zhang, S. Hong, F. Xing, B. Dong, Visualized tracing of crack self-healing features in cement/microcapsule system with X-ray microcomputed tomography, *Constr. Build. Mater.* 179 (2018) 336–347, <https://doi.org/10.1016/j.conbuildmat.2018.05.193>.
- [30] P. Risdanareni, J. Wang, N. Boon, N. De Belie, Alkali activated lightweight aggregate as bacterial carrier in manufacturing self-healing mortar, *Constr. Build. Mater.* 368 (2023) 130375, <https://doi.org/10.1016/j.conbuildmat.2023.130375>.
- [31] L. Schröer, Chapter 5. Examining alteration processes induced by heterotrophic bacteria, 2021.
- [32] K. Van Tittelboom, N. De Belie, Self-healing in cementitious materials - a review, *Mater.* 6 (2013) 2182–2217, <https://doi.org/10.3390/ma6062182>.
- [33] F. Grosso Giordano, M. Brunin, N. Boon, N. De Belie, On the use of non-destructive testing for the measurement of self-healing in lime-based mortars, *Mater. Today Proc.* (2023), <https://doi.org/10.1016/j.matpr.2023.07.367>.